JOURNAL OF CATALYSIS **176,** 545–551 (1998)
ARTICLE NO. CA982045

Alkylation of Isobutane with 1-Butene on Zeolite Beta

R. Loenders, P. A. Jacobs, and J. A. Martens[1]

Centrum voor Oppervlaktechemie en Katalyse, Kardinaal Mercierlaan 92, B-3001 Heverlee, Belgium

Received December 16, 1997; revised February 16, 1997; accepted February 16, 1997

Alkylation of isobutane with 1-butene was carried out in the liquid phase at 353 K on beta zeolite catalyst samples with varying framework Si/Al ratios and particle sizes. The specific external surface area determined with nitrogen physisorption and t-plot analysis is the key parameter to rationalize alkylation activity and stability. The catalytic activity of zeolite beta samples with specific external surface areas smaller than ca 280 $m^2\ g^{-1}$ suffers from intracrystalline diffusional limitations. The critical particle size to avoid diffusional limitations is estimated at 14 nm. In the absence of diffusional limitations, the alkylate yield obtained during the catalyst lifetime is proportional to the number of Brönsted acid sites in the zeolite and amounts to ca 3 kg $mole^{-1}$, irrespective of the acid site density. The deactivation of the samples is explained by a site coverage model.

INTRODUCTION

Driven by environmental concerns, the levels of olefins and aromatics tolerated in gasoline are continuously decreasing. To cope with the volume reduction of the total gasoline pool and with the losses in octane numbers, alkylation processes converting lower alkenes and isobutane into branched isoalkanes with high octane numbers have become important gasoline production processes (1). As the current alkylation technology makes use of homogeneous acid catalysts such as hydrofluoric and sulfuric acid, there is considerable interest in the development of alternative technology based on heterogeneous catalysts (2).

With heterogenized gaseous and liquid strong acids (3–6), the risk of leaching of the "immobilized" acid always remains, requiring continuous addition of fresh acid. The development of true solid acid catalysts and appropriate reactor technology for these demanding alkylation reactions is a challenge. Strongly acidic solids including chlorinated alumina (7), acid resins (8), sulfated zirconia (9), and acid zeolites (10–22) have been evaluated as potential catalysts.

In literature, zeolite alkylation catalysts have received much attention (10–22). Whereas medium pore zeolites are rather inactive as a result of unfavorable molecular shape selectivity (13, 17, 18), large pore zeolites invariably show rapid deactivation (10–16, 18–22). Obvious reasons for fast deactivation of zeolite catalysts are pore blockage and poisoning of active sites with heavy reaction products (23). Simpson *et al.* (24) modeled transient conversion data during alkylation of isobutane with trans-2-butene over ultrastable Y zeolite and proposed a site-coverage deactivation model. In this model, the kinetic constant of hydride transfer to C_8 alkylcarbenium ions was found to be too slow compared to that of olefin addition to the same carbocation, leading to a deposition of heavy oligomers on the individual acid sites. Weitkamp and Maixner (25) characterized deactivated lanthanum Y zeolites using ^{13}C MAS NMR and IR spectroscopy and concluded that the carbonaceous deposits formed in alkylation reactions at 353 K had a H/C ratio of 1.8, which is slightly below that of an alkene.

Zeolite beta has been found to deactivate less rapidly compared to faujasite zeolites (18, 20). Corma *et al.* (19) synthesized zeolite beta samples according to various recipes and were able to correlate the catalytic activity and time-on-stream stability of a zeolite beta sample with the resistance to framework dealumination upon calcination and with its residual concentration of strong acid sites found in their collection of samples. Unverricht *et al.* (20) used zeolite beta samples with Si/Al ratios of 12, 19, 70, and 90 and reported an optimum activity and stability for the sample with Si/Al ratio of 19. Although the critical physico-chemical properties governing activity and stability remain incertain, it appears that activity and stability of zeolite beta samples are linked, as the most active samples retain their activity for a longer period. Diffusional limitation of the alkylation reaction rate is severe at the low reaction temperatures at which the liquid phase processes even on ultrastable Y type zeolites (24).

In the present work we investigated the alkylation of isobutane with 1-butene using two sets of carefully prepared and characterized zeolite beta samples, either with similar texture and varying acid site density, or with varying texture. These samples allowed us to determine the deactivation mechanism in zeolite beta, to evaluate diffusional limitations, and to identify the critical parameters limiting the zeolite beta catalyst lifetime.

[1] Corresponding author. E-mail: johan.martens@agr.kuleuven.ac.be.

0021-9517/98 $25.00

EXPERIMENTAL

Zeolite Beta Samples

The origin, modification, and physico-chemical properties of the zeolite beta samples are shown in Table 1. Beta PQ1 was dealuminated with hydrochloric acid, by slurrying 5 g of the sample in 100 ml solution of 0.1 *N* HCl (Beta PQ0.1N) or 0.5 *N* HCl (Beta PQ0.5N) for 2 h at room temperature. The samples were washed with distilled water until the pH of the slurry was neutral, dried, and calcined at 823 K in a muffle furnace. All zeolite beta samples were cation exchanged with NH_4Cl using a 0.5 *M* NH_4Cl solution for 12 h under reflux conditions to remove cationic aluminum species dislodged from the framework as well as residual alkali metal cations.

The total and framework aluminum content of the samples (Table 1) was determined by quantitative ^{27}Al MAS NMR on a Bruker MSL 400 instrument, at a frequency of 104.3 MHz, a rotor spinning frequency of 11 kHz, using 0.5 *M* aqueous $Al(NO_3)$ as chemical shift standard, and Beta PQ1 with total Si/Al ratio of 12.8 and framework Si/Al ratio of 17.3 as aluminum concentration standard. The total aluminum content is obtained by the integration of the entire ^{27}Al MAS NMR intensity, the framework aluminum content by integration of the signal intensity from 10 to 70 ppm. The number of scans was 6000, the pulse length 0.61 μs and the repetition time 0.1 s. Before use, all samples were hydrated to constant humidity by storing them over a saturated solution of aqueous NH_4Cl.

Infrared spectra were recorded on a Nicolet 730 FTIR spectrometer. The zeolite powders were compressed into self-supporting wafers and placed in a vacuum chamber equipped with CaF_2 windows, mounted in the spectrometer. The zeolite wafers were heated overnight in vacuum at 733 K, the spectra were recorded at room temperature. For the quantification of the hydroxyl concentrations, the absorbances were recalculated to a wafer thickness of 1 mg of dry sample per cm^2 of wafer surface area using Beers law. A straight baseline tangential to the spectra at 3800 and 3000 cm^{-1} was used for quantification purposes.

Nitrogen adsorption isotherms at 77 K were recorded on degassed samples with an Omnisorp 100 instrument from Coulter operated in the continuous flow mode. The isotherms were transformed into t-plots according to the method of Lippens and de Boer (28). For adsorbed film thicknesses between 0.3 and 0.9 nm, the t-plots were linear (R value of at least 0.99). Micropore volumes and specific external surface areas given in Table 1 were derived from the t-plot curve, using the intercept with the Y axis and the slope of the straight line, respectively.

Reactor Setup

Seven-tenths grams of catalyst pellets with diameters of 0.5 to 0.8 mm, obtained by compressing the powder into tablets, crushing, and sieving, were loaded in a stainless steel reactor tube with internal diameter of 1 cm and a length of 10 cm. The catalyst bed was fixed between two plugs of quartz wool and the remaining empty volume filled with glass beads of the same diameter. The catalysts were pretreated *in situ* in a flow of oxygen gas of 100 ml/min. The temperature profile for the pretreatment comprised heating at a rate of 2 K/min to 383 K, an isothermal period of 2 h, a second heating step to 723 K at 2 K/min and another isothermal period of 5 h. The reactor was cooled to 353 K and the activated catalyst was contacted first with hexane, pumped through the reactor at a pressure of 3 MPa

TABLE 1

Characterization of Zeolite Beta Samples

Sample	Origin/original form	Modifications	Si/Al ratio		Specific mesopore surface area (m^2/g)[d]	Micropore volume (ml/g)[d]
			Total	Framework		
Beta U	Ueticon/H-form	NH_4-exchange	9.9[b]	13[b]	284	0.19
Beta PQ1	PQ (CP811)/H-form	NH_4-exchange	12.8[a]	17.3[b]	361	0.17
Beta PQ0.1N	Beta PQ1	Acid leaching 0.1N HCl/NH_4-exchange	24.6[b]	33[b]	370	0.17
Beta PQ0.5N	Beta PQl	Acid leaching 0.5N HCl/NH_4-exchange	57.7[b]	77[b]	373	0.16
Beta PQ2	PQ (CP806) as-synthezised	Calcination at 550°C/NH_4-exchange	12.5[b]	16.7[b]	346	0.17
Beta C	Synthezised according to (26) ex B1	Calcination at 550°C/NH_4-exchange	7.5[c]	n.d.	84	0.21
Beta F	Synthezised according to (27) ex 5	Calcination at 550°C/NH_4-exchange	12[c]	n.d.	43	0.15

[a] Determined by chemical analysis, data from manufacturer.
[b] Determined by quantitative ^{27}Al MAS NMR.
[c] Determined by chemical analysis, data from original literature.
[d] Determined with nitrogen physisorption at 77 K and t-plot analysis.

using a Waters 590 HPLC pump to establish liquid phase conditions in the reactor. The feedstock consisting of an isobutane/1-butene mixture with a molar ratio of 100/1, containing 1 wt% of nonane as internal standard was delivered to the reactor using a mass flow controller for liquids (Rosemount/Brooks Instruments B.V., type 5881) from a storage vessel pressurized at 3.5 MPa with nitrogen. The WHSV (weight hourly space velocity) of the liquid feedstock was 53.5 h^{-1}.

The reaction products were analyzed using a high resolution gas chromatograph with F.I.D. detector (HP 5890 series II) and WCOT fused silica column from Chrompack (CP-Sil-5-CB with a film thickness of 5.49 μm, and a length of 50 m). The reaction product stream was sampled at high pressure using a liquid sampling valve with an internal volume of 0.1 μl. Collection and temporary storage of product samples is achieved using a 10-way valve with four external loops. A flow scheme of the unit is shown in Fig. 1.

Catalytic Definitions

As double bond shift in 1-butene was found to be very rapid, in the reaction conditions, the C4 double bound isomers are considered as unconverted feed, denoted as "butene." The butene conversion, X_b, has been calculated from the integrated GC peak areas, A_i, using the expression

$$X_b\,(\%) = \frac{\frac{W_b^f}{W_s^f} - \frac{\sum A_b^p}{A_s^p}}{\frac{W_b^f}{W_s^f}} 100$$

in which W stands for weight fraction; the subscripts b and s refer to butene and internal standard, respectively; the superscripts f and p refer to feedstock and reaction products, respectively.

The selectivity for a specific product fraction i, S_i, is defined as the number of moles of product i produced per mole of butene converted. It is calculated according to the formula

$$S_i\,(\%) = \frac{\frac{W_s^f}{MW_i}\frac{A_i}{A^s}}{\frac{W_b^f}{MW_b}\frac{X_b}{100}}\frac{CN_i}{4} 100$$

in which CN_i and MW_i are the carbon number and the molecular weight of the product molecules i.

The CN of the reaction products was always 5 or higher (C_5^+). The sum of selectivity's ($\sum S_i$) in percentage corresponds to the number of moles of C_5^+ products formed per mole of butene converted, multiplied by 100. Pure alkylation results in a sum of selectivity's of 200%, while pure oligomerization gives a sum of selectivity's of only 100%. Sums of selectivity's lower than 100% are indicative of a deficiency in the hydrocarbon mass balance and retention of heavy products on the catalyst.

Since all oligomerization products cannot be distinguished from alkylation products, it was not possible to determine the alkylate yield exactly. The alkylate yield (Y) used in this work is defined as the yield of C_5^+ products (g) obtained per unit weight of catalyst (g), integrated over the catalyst lifetime from the start of the catalytic experiment until a time τ at which the sum of selectivity's dropped below 120%:

$$Y = \int_0^\tau \left(\sum S_i/100\right)(X_b/100)(F_b/W_c)\,dt.$$

The 1-butene fed (F_b) and the catalyst weight (W_c) are expressed in grams.

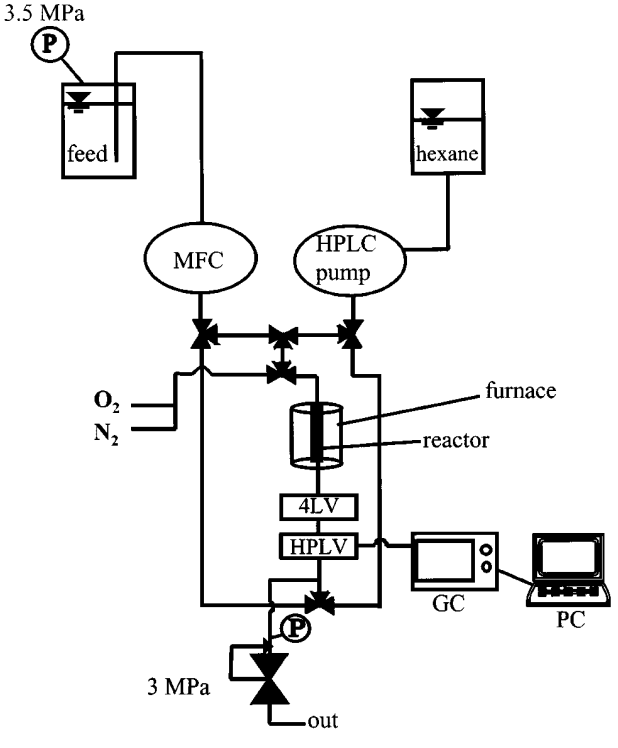

FIG. 1. Flow scheme of the liquid phase alkylation reaction unit (MFC = mass flow controller for liquids; 4LV = 4 loop valve; HPLV = high pressure liquid valve for sampling, GC = gas chromatograph, and PC = personal computer).

RESULTS AND DISCUSSION

Characterization of Beta Samples

The hydroxyl spectra of zeolite beta catalysts (Fig. 2), all show typical hydroxyl bands: an intense silanol band at ca 3745 cm^{-1}, bridging hydroxyls at ca 3610 cm^{-1}, a weak very high frequency (VHF) band at 3780 cm^{-1}, and a weak signal at 3660 cm^{-1}. In the literature, the bands at 3780 and 3660 cm^{-1} are assigned to hydroxyls linked to aluminum atoms dislodged from the framework (29–31). The intensities of the VHF and 3660 cm^{-1} bands are lower in sample

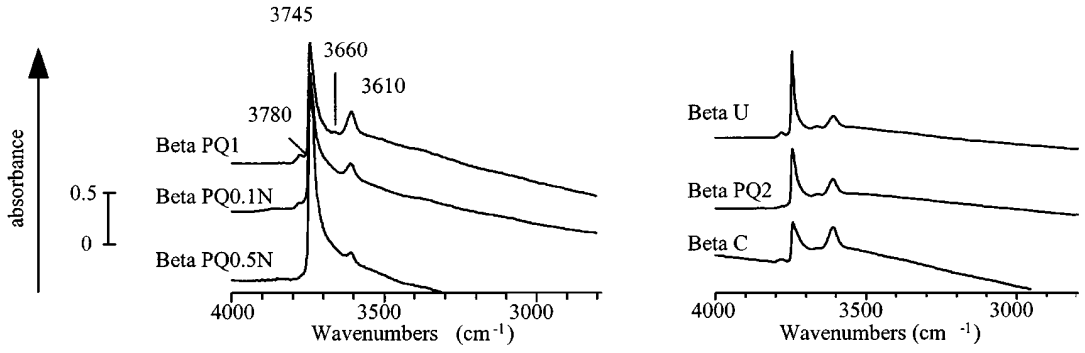

FIG. 2. IR hydroxyl stretching spectra of beta zeolite catalysts.

Beta PQ2, compared to the two other commercial samples. In sample beta C, the relative intensities of the hydroxyl bands are different. The higher intensity of the stretching vibration band of the bridging hydroxyls (3610 cm^{-1}) is due to the higher aluminum content of sample beta C (Si/Al ratio of 7.5). In beta C, the intensities of the silanol vibration band and, especially, of the band at 3660 cm^{-1}, are significantly lower compared to the commercial samples.

Dealumination of Beta PQ1 with HCl leads to a gradual reduction of the intensity of the 3780, 3660, and 3610 cm^{-1} bands and to an increase of the intensity of the silanol vibration. This dealumination was also evidenced with quantitative ^{27}Al MAS NMR. The framework Si/Al ratio increases from the value of 17.3 for the parent sample to 33 and 77 after treatment with 0.1 N and 0.5 N aqueous HCl, respectively (Table 1). A plot of the framework Al content determined with ^{27}Al MAS NMR against the absorbance at 3610 cm^{-1} (Fig. 3) teaches that the concentration of bridging hydroxyl groups in the zeolite is proportional to the concentration of framework aluminum atoms determined with ^{27}Al MAS NMR.

The morphology of the zeolite beta samples evidenced with scanning electron microscopy corresponds to ill-defined particles. The particle size was therefore characterized with nitrogen physisorption and t-plot analysis. The specific surface area in meso- and macropores derived from the slope of the t-plots is a measurement of the external specific surface area of the elementary microporous particles. The beta samples studied represent a variation of specific external surface areas from 43 $m^2\ g^{-1}$ up to 373 $m^2\ g^{-1}$ (Table 1). The dealumination of the Beta PQ sample with HCl did not significantly alter the texture (Table 1).

Alkylation of Isobutane with 1-Butene on Zeolite Beta

The change of butene conversion with time-on-stream, expressed as the weight of 1-butene per unit weight of catalyst, is shown in Fig. 4 for Beta PQ1, Beta PQ0.1N, and Beta PQ0.5N. The butene conversion decreases with time-on-stream due to catalyst deactivation. On sample Beta PQ0.5N, even initially, butene was not entirely consumed. The catalytic activity of zeolite beta is decreased by dealumination.

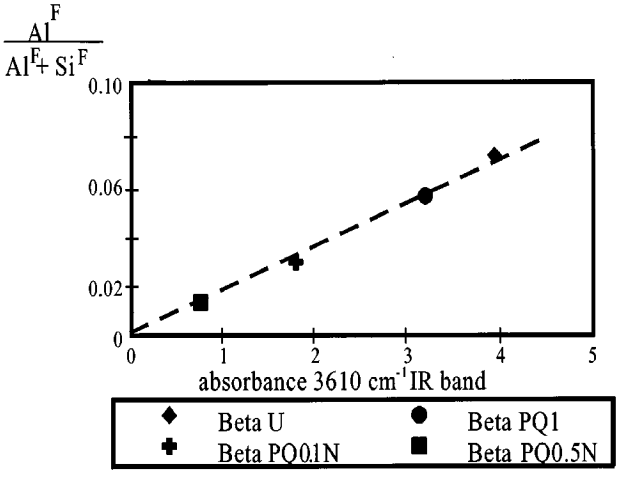

FIG. 3. Framework Al/(Al + Si) atomic ratio, determined with ^{27}Al MAS NMR versus IR absorbance at 3610 cm^{-1} (arbitrary units).

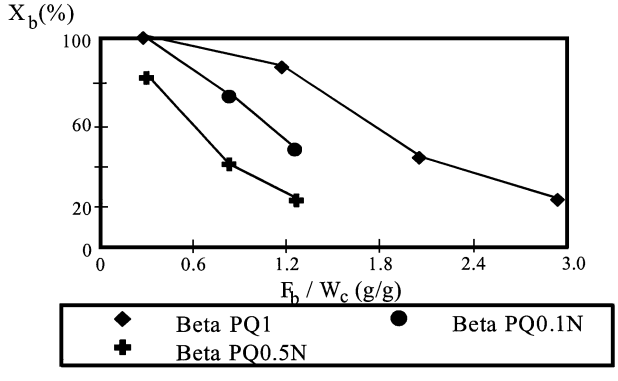

FIG. 4. Butene conversion obtained over Beta PQ1, Beta PQ0.1N, and Beta PQ0.5N samples versus its amount fed per unit weight of catalyst (g/g). Reaction conditions: temperature = 353 K; pressure = 3 MPa; isobutane/butene (molar) ratio = 100.

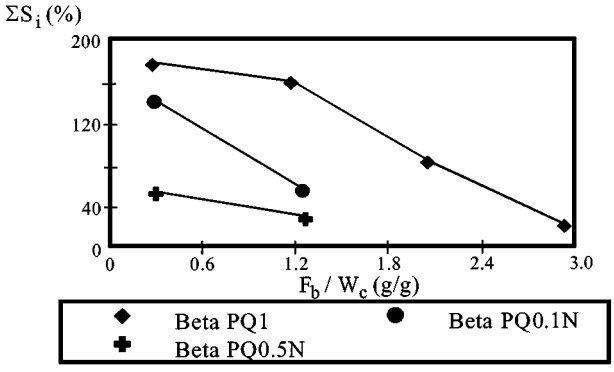

FIG. 5. Sum of Selectivity's obtained over Beta PQ1, Beta PQ0.1N, and Beta PQ0.5N samples versus the amount of butene fed per unit weight of catalyst (g/g) (experiments of Fig. 4).

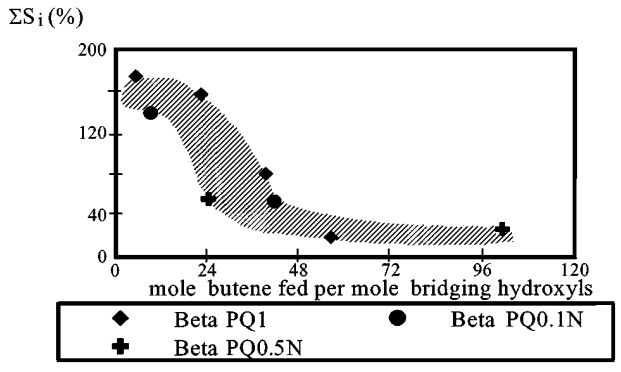

FIG. 7. Sum of selectivity's obtained over Beta PQ1, Beta PQ0.1N, and Beta PQ0.5N samples versus the number of moles of butene fed per mole of bridging hydroxyls in the zeolite (experiments of Fig. 4).

The sum of selectivity's obtained with the three catalysts is plotted against time-on-stream in Fig. 5. On the parent zeolite beta, initially the sum of selectivitys is 180%, indicative of almost pure alkylation. The decreasing sum of selectivitys indicates that oligomerization becomes gradually more important. Hence, deactivation is accompanied by a decrease in alkylation selectivity, a phenomenon commonly observed with zeolites (9, 12, 13, 18). Dealumination of zeolite beta leads systematically to lower sums of selectivity's.

However, when the time-on-stream is expressed on bridging hydroxyl (or framework aluminum) basis, the experimental butene conversion data (Fig. 6) and the sum of selectivitys (Fig. 7) can be fitted to a common curve for the three beta samples. It can be concluded that the number of butene turnovers performed by an individual acid site in beta zeolites under the present reaction conditions is independent of the aluminum content. Furthermore, it indicates that catalyst deactivation is caused by a deactivation of the individual active sites of these beta zeolites, rather than by a pore-plugging mechanism. The latter would not yield unique curves. The alkylate yield obtained during the catalyst lifetime corresponds to ca 3 kg per mole framework aluminum, irrespective of the aluminum content of the zeolite. A similar sequential deactivation model has been proposed by Simpson *et al.* for ultrastable Y zeolites (24). Such acid site poisoning finds a rational basis in the reaction mechanisms of acid catalyzed alkylation and oligomerization (32). C_8 alkylcarbenium ions obtained after addition of butene to C_4 alkylcarbenium ions either abstract a hydrogen atom from isobutane and desorb as an isoalkane, or react with butene molecules to become large oligomers irreversibly adsorbed on the acid site. Corma *et al.* (22) have investigated the influence of the Si/Al ratio of USY zeolites on the isobutane/butene alkylation and concluded that a high aluminum content was favorable for the activity, selectivity, and stability of the catalyst, as presently observed for beta zeolites. Its assignment to an enhanced hydride transfer capacity of Al-rich zeolites (22) does not hold for the present series of high-silica beta zeolites, since the activity and stability per site is independent of the aluminum content.

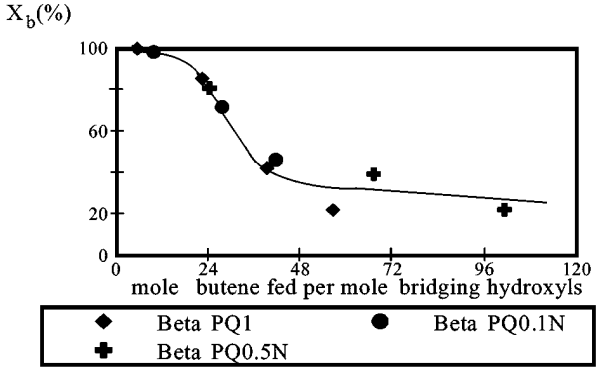

FIG. 6. Butene conversion obtained over Beta PQ1, Beta PQ0.1N, and Beta PQ0.5N samples versus the number of moles of butene fed per mole of bridging hydroxyls in the zeolite (experiments of Fig. 4).

With the different beta samples tested, the reaction product distribution, determined at high butene conversion is very similar and not dependent on aluminum content, nor on particle size (Table 2). This observation further supports the proposed unique activity and stability of the acid sites in beta zeolites. Corma *et al.* (34) reported sample dependent product distributions for isobutane/2-butene alkylation using an alkane/alkene ratio of 15 and at 90% alkene conversion. Under those reaction conditions, alkylation is accompanied by some oligomerisation, depending on the nature of the zeolite beta samples.

Comparison of zeolite beta samples with different particle sizes and similar Al contents was useful to estimate the occurrence of diffusional limitation. The changes of butene conversion and alkylate yield with time-on-stream of these beta samples are reported in Figs. 8 and 9, respectively. The highest activity, stability, and alkylation yield is

TABLE 2

Product Distributions, Samples Taken after 0.3 g of Butene Fed per 1 g of Catalyst

Conversion (%)	Beta U 100	Beta PQ1 100	Beta PQ2 100	Beta C 99.4	Beta F 92.3
Product fractions (wt%)					
C5	5.4	6.5	7.9	6.3	6.6
C6	3.5	3.9	2.9	3.3	3.3
C7	6.3	6.9	6.5	6.1	6.0
C8	71.8	68.5	66.6	70.1	70.7
C9+	12.9	14.2	16.2	14.1	13.4
C8 distribution (%)					
Monobranched C8	1.9	1.6	2.1	1.4	1.3
Dibranched C8	15.0	15.9	15.9	15.0	15.4
2,2,4-trimethyl pentane	49.5	48.2	47.9	49.1	47.9
2,2,3-trimethyl pentane	7.9	6.9	7.6	7.0	6.2
2,3,4-trimethyl pentane	13.6	17.1	16.6	17.1	18.2
2,3,3-trimethyl pentane	11.7	10.2	9.5	9.6	10.5

obtained with beta U. With this sample, the sum of selectivity's reaches initially a value close to 200%, indicative of pure alkylation. Beta PQ1 and Beta PQ2 are slightly less active. Beta C and Beta F are much less active. Even initially, the butene conversion over Beta F sample is incomplete. These differences in catalytic activity and stability among the samples do not reflect in every case the differences in aluminum content or available micropore volumes as shown by the relationship between the yield of alkylate per active site and the external specific surface area (Fig. 10). Up to an external surface area of ca 280 $m^2\ g^{-1}$, the alkylate yield is proportional to the available external surface area. This can be explained by the existence of severe intraparticle diffusional limitation, the catalytic activity being concentrated in the outer rim of the particles. For larger external surface areas,the alkylate yield per site does not depend on the external surface area and intracrystalline

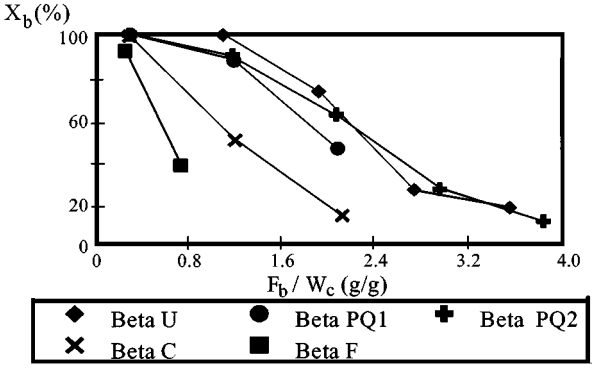

FIG. 8. Butene conversion over the zeolite beta samples versus its amount fed per unit weight of catalyst (g/g). Reaction conditions: temperature = 353 K; pressure = 3 MPa; isobutane/butene (molar) ratio = 100.

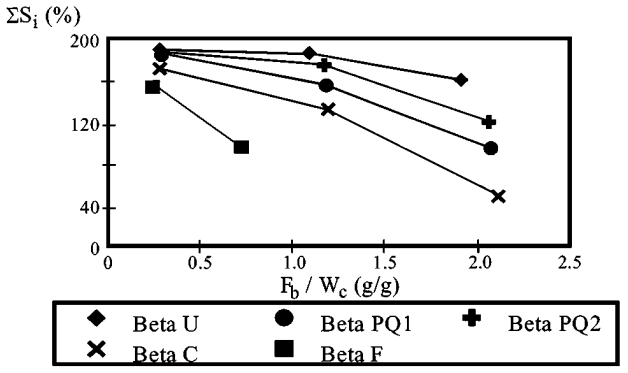

FIG. 9. Sum of Selectivity's obtained over the zeolite beta samples versus the amount of butene fed per unit weight of catalyst (g/g) (experiments of Fig. 8).

diffusion is no longer rate limiting. This situation is encountered in samples Beta U, Beta PQ1, and Beta PQ2. In these samples the highest possible number of effective turnovers is obtained. This maximum corresponds to ca 3 kg of alkylate per mole of acid sites. The transition from the regime of diffusional limitation to kinetic limitation seems to occur at an external surface area around 280 $m^2\ g^{-1}$. Assuming a cubic shape for the zeolite particles and using a density of 1.5 g/cm^3 for zeolite beta (33), this critical value for the specific external surface area corresponds to particles of 14 nm.

CONCLUSIONS

In the alkylation of isobutane with 1-butene at 353 K, diffusional limitations are absent in beta zeolites with specific external surface areas larger than ca 280 $m^2\ g^{-1}$, corresponding to particle sizes smaller than 14 nm. Such small zeolite beta particles deactivate by a mechanism of coverage of the individual acid sites with bulky oligomeric reaction products. The individual acid sites perform an identical number of catalytic turnovers before deactivation and produce, irrespective the acid site density, ca 3 kg of alkylate

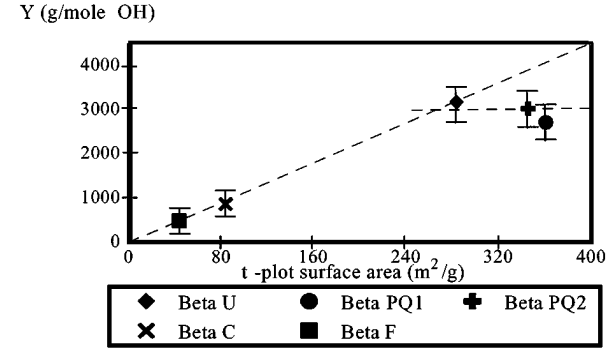

FIG. 10. Alkylate yield, expressed in grams per mole bridging hydroxyls, obtained over the different zeolite beta samples, versus the t-plot surface area of these samples (experiments of Fig. 8).

per mole of sites. The present study reveals that the only way to enhance the activity and stability of zeolite beta for isobutane alkylation is by increasing the aluminum content of zeolite beta nanoparticles. Deactivation cannot be avoided, however.

ACKNOWLEDGMENTS

This work is part of the Ph.D. of R.L., sponsored by Total Raffinage Distribution. A research grant from the Flemish government within the G.O.A. frame is highly appreciated.

REFERENCES

1. Hatch, L. F., and Matar, S., From hydrocarbons to petrochemicals, *Hydrocarbon Processing*, May 1977–May 1980.
2. Corma, A., and Martinez, A., *Catal. Rev. Sci. Eng.* **35**(4), 483 (1993).
3. Child, J. E., Chou, T. S., Huss, A., Jr., Kennedy, C. R., Ragonese, F. P., and Tabak, S. A., U.S. Patent 4,956,518 (1990).
4. Cooper, M. D., King, D. L., and Sanderson, W. A., WO 92/04977 (1992).
5. Huss, A., Jr., and Johnson, I., D., U.S. Patent 5,221,777 (1993).
6. Huang, T. J., U.S. Patent 4,384,161 (1983).
7. Goupil, J. M., Poirier, J. L., and Cornet, D., *Catal. Lett.* **31**, 121 (1995).
8. Rørvik, T., Dahl, I. M., Mostad, H. B., and Ellestad, O. H., *Catal. Lett.* **33**, 127 (1995).
9. Corma, A., Martinez, A., and Martinez, C., *J. Catal.* **149**, 52 (1994).
10. Kirsch, W. F., Potts, J. D., and Barmby, D. S., *presented before the* "Div. Petro. Chem. ACS, San Fransico, 1968," p. 153.
11. Garwood, W. E., and Venuto, P. B., *J. Catal.* **11**, 175 (1968).
12. Weitkamp, J., *in* "Proc. 5th Int. Confer. on Zeolites, 1980."
13. Chu, Y. F., and Chester, A. W., *Zeolites* **6**, 195 (1986).
14. Juguin, B., Raatz, F., and Marcilly, C., French Patent 2,631,956 (1988).
15. Huss, A., Jr., Kirker, G. W., Kevill, K. M., and Thomson, R. T., U.S. Patent 4,992,615 (1991).
16. Stöcker, M., Mostad, H., and Rørvik, T., *Catal. Lett.* **28**, 203 (1994).
17. Weitkamp, J., and Jacobs, P. A., *in* "Proc. 10th Int. Congress on Catalysts, 1992."
18. Corma, A., Martinez, A., and Martinez, C., *Catal. Lett.* **28**, 187 (1994).
19. Corma, A., Gomez, V., Martinez, A., *Appl. Catal. A: General* **119**, 83 (1994).
20. Unverricht, S., Ernst, S., and Weitkamp, J., *Stud. Surf. Sci. Catal.* **84**, 1693 (1994).
21. Mesters, C. M. A. M., Van Bruggel, Th. M., de Groot, C., de Jong, K. P., Peferoen, D. F. G., *in* "Proc. Europa Cat II Sept. 1995, Maastricht, 1995," p. 773.
22. Corma, A., Martinez, A., and Martinez, C., *J. Catal.* **146**, 185 (1994).
23. Guisnet, M., and Magnoux, P., "Zeolite Microporous Solids: Synthesis, Structure and Reactivity" (Derouane *et al.*, Eds.). Kluwer Acad., Amsterdam, 1992.
24. Simpson, M. F., Wei, J., and Sundaresan, S., *Ind. Eng. Chem. Res.* **35**, 3861 (1996).
25. Weitkamp, J., and Maixner, S., *Zeolites* **7**, 6 (1987).
26. Perez-Pariente, J., Martens, J. A., and Jacobs, P. A., *Appl. Catal.* **31**, 35 (1987).
27. Caullet, Ph., Guth, J. L., Faust, A. C., Raatz, F., Joly, J. F., and Deves, J. M., EU Patent 0,419,334 A1 (1991).
28. Lippens, B. C., and de Boer, J. H., *J. Catal.* **4**, 319 (1965).
29. Bougeat-Lami, E., Massiani, P., Di Renzo, F., Espiau, P., Fajula, F., and Des Courières, T., *Appl. Catal.* **72**, 139 (1991).
30. Jia, C., Massianin, P., and Bartomeuf D., *J. Chem. Soc. Faraday Trans.* **89**, 3659 (1993).
31. Kiricsi, I., Flego, C., Pazzuconi, G., Parker, W. O., Millini, R., Perego, C., and Bellusi, G., *J. Phys. Chem.* **98**, 4627 (1994).
32. Schmerling, L., *J. Am. Chem. Soc.* **66**, 1472 (1944).
33. Meier, W. M., Olson, D. H., and Baerlocher, Ch., "Atlas of Zeolite Structure Types," 4th ed., Zeolites, Vol. 17, pp. 1–230. Butterworth, Guildforth, UK, 1996.
34. Corma, A., Martinez, A., Arroyo, P. A., Monteiro, J. L. F., and Sousa-Aguiar, E. F., *Appl. Catal. A: General* **142**, 139 (1996).